Cellular and Molecular Life Sciences (2018) 75:2059–2073
https://doi.org/10.1007/s00018-017-2722-7

ORIGINAL ARTICLE

The SH3-binding domain of Cx43 participates in loop/tail interactions critical for Cx43-hemichannel activity

Jegan Iyyathurai[1] · Nan Wang[2] · Catheleyne D'hondt[1] · Jean X. Jiang[3] · Luc Leybaert[2] · Geert Bultynck[1]

Received: 10 April 2017 / Revised: 24 November 2017 / Accepted: 27 November 2017 / Published online: 7 December 2017

Abstract

Connexin 43 (Cx43) hemichannels establish local signaling networks via the release of ATP and other molecules, but their excessive opening may result in cell death. Hence, the activity of Cx43-hemichannels ought to be critically controlled. This involves interactions between the C-terminal tail (CT) and the cytoplasmic loop (CL), more particularly the L2 domain within CL. Previous work revealed an important role for the last nine amino acids of the Cx43 CT by targeting the L2 domain, as these nine amino acids were sufficient to restore the activity of CT-truncated Cx43-hemichannels. However, we discovered that deletion of the last 19 amino acids of the CT only partially lowered the binding to the L2 domain, indicating that a second L2-binding region is present in the CT. We here provide evidence that the SH3-binding domain is another CT region that targets the L2 domain. At the functional level, the SH3-binding domain was able to restore the activity of CT-truncated Cx43-hemichannels and alleviate the inhibition of full-length Cx43-hemichannels by high intracellular Ca^{2+} concentration ($[Ca^{2+}]_i$) as demonstrated by various approaches including patch clamp studies of unitary Cx43-hemichannel activity. Finally, we show that in full-length Cx43-hemichannels, deletion of either the SH3-binding domain or the CT9 region suppresses the hemichannel activity, while deletion of both domains completely annihilates the hemichannel activity. These results demonstrate that the Cx43 SH3-binding domain, in addition to the CT9 region, critically controls hemichannel activity at high $[Ca^{2+}]_i$, which may be involved in pathological hemichannel opening.

Keywords Connexin · Hemichannels · Gap junctions · Calcium · Ca^{2+}-wave propagation · Intercellular communication · ATP release · Electrophysiology · Single channel recordings

Introduction

Connexins play a critical role in a variety of cellular and physiological processes by forming hemichannels and gap junctions that permit intercellular communication. The functional channel unit is based on a hexameric structure, a connexon, which can function as unopposed channels, i.e., hemichannels, as well as head-to-head-docked channel complexes in gap junctions. One of the major connexin isoforms is the 43-kDa connexin, connexin 43 (Cx43), which is expressed in a variety of cell types and tissues, including cardiomyocytes, astrocytes, endothelial cells, osteocytes and many more [1]. Gap junctions are important for the direct passage of low molecular weight molecules (< 1.5 kDa) between neighboring cells. Hemichannels mediate the exchange of signaling molecules with the extracellular environment, including the release of ATP, glutamate and the influx of various ions including Na^+ and Ca^{2+} [2]. While gap junctions and hemichannels are formed by the

Electronic supplementary material The online version of this article (https://doi.org/10.1007/s00018-017-2722-7) contains supplementary material, which is available to authorized users.

Luc Leybaert and Geert Bultynck share the last authorship.

✉ Geert Bultynck
geert.bultynck@kuleuven.be

[1] Laboratory of Molecular and Cellular Signaling, Department Cellular and Molecular Medicine, KU Leuven, Campus Gasthuisberg O/N-1 Bus 802, Herestraat 49, 3000 Louvain, Belgium

[2] Physiology Group, Department of Basic Medical Sciences, Faculty of Medicine and Health Sciences, Ghent University, De Pintelaan 185, 9000 Ghent, Belgium

[3] Department of Biochemistry and Structural Biology, University of Texas Health Science Center, San Antonio, TX, USA

same building blocks, they seem to be fundamentally different in their regulation at the molecular and functional level [3]. In basal conditions, gap junctions (or at least a fraction of them) are open, while hemichannels mainly reside in a closed state [4]. The latter prevents the loss of ionic, energetic and metabolic gradients, and thus is essential for cell survival [2, 5]. A prominent role for intramolecular interactions of the C-terminal tail (CT) with the cytoplasmic loop (CL) has been described to affect the activity of both gap junctions and hemichannels, but with an opposite effect on channel function [3]. Such loop/tail interaction was shown to be responsible for the closure of Cx43 gap junctions, an event that occurs under conditions of ischemia, metabolic inhibition or intracellular acidification [6]. As a consequence, the closure of cardiac gap junctions after ischemia-reperfusion is responsible for the compromised electrical and thus rhythmic and contractile properties of the heart. Gap junctions formed by Cx43 proteins lacking the CT are resistant to acidification-induced closure [6]. These insights have been exploited to develop peptides and peptidomimetic small molecules that bind the CT and prevent loop/tail interactions, thereby sustaining Cx43 gap junction activity despite intracellular acidification [3, 7, 8]. In contrast, loop/tail interactions are essential for bringing hemichannels to an "available to open" state from which actual opening can be triggered by low extracellular Ca^{2+} concentration ($[Ca^{2+}]_e$), modest intracellular Ca^{2+} concentration ($[Ca^{2+}]_i$) rises ($\leq$ 500 nM) or by membrane depolarizations above + 30 mV (reviewed in Wang et al. [9]). Strikingly, hemichannels formed by Cx43 proteins lacking the CT are refractive to opening in response to various stimuli [10]. The activity of $Cx43^{M239}$-based hemichannels (Cx43-truncated at amino acid 239) can be restored by re-adding the last nine amino acids of the CT of Cx43 (CT9) as a cell-permeant, synthetic peptide (TAT-CT9) [10]. The mechanism involved a direct interaction between the CT9 region and the L2 domain located on the CL (Fig. 1). While Cx43-hemichannel opening is promoted by modest (~ 500 nM) $[Ca^{2+}]_i$ elevation, higher concentrations (~ 1 µM and above) act to close the channels again [11, 12]. Interestingly, loss of loop/tail interaction seemed to underlie the inhibition of Cx43-hemichannel activity by 1 µM $[Ca^{2+}]_i$ via a mechanism that involves the activation of the actomyosin cytoskeleton. Indeed, TAT-CT9 as well as (−)-blebbistatin, a myosin II ATPase inhibitor blocking myosin II in an actin-detached state [13], prevented the Cx43-hemichannel inhibition by high $[Ca^{2+}]_i$ [14]. This interaction was based on the presence of negatively charged Asp residues in the CT9 region of Cx43 [15]. As a consequence, TAT-L2 inhibited the opening of Cx43-hemichannels, but not Cx43 gap junctions. In further work, the activity of L2 could be pinned down to a nine amino acid sequence, named Gap19. Gap19, a stretch containing many positively charged amino acids,

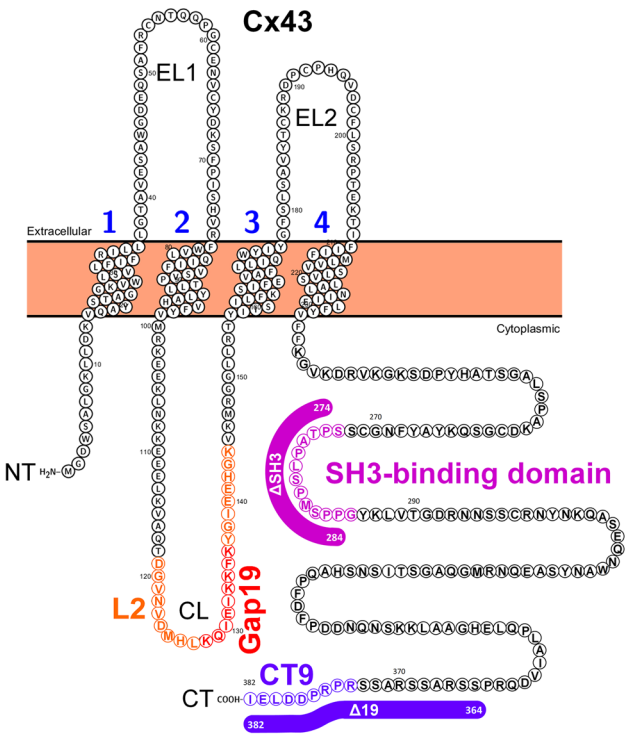

Fig. 1 Schematic representation of Cx43-protein sequence depicting the domains relevant for this study. Schematic illustration of the human Cx43 protein sequence (protein accession number used: P17302) using the Protter protein-visualization tool (http://wlab.ethz.ch/protter/start/; [37]), which represents one building block of the hexameric hemichannel. The four transmembrane domains are numbered. The cytoplasmic loop (CL), which harbors the L2 and Gap19 region, and the cytoplasmic tail (CT), which harbors the SH3-binding domain and the CT9 region, are indicated. Also, the amino acid regions that were deleted in Cx43 or Cx43-CT to generate full-length Cx43 mutants: $Cx43^{\Delta SH3}$, $Cx43^{\Delta 19}$, $Cx43^{\Delta SH3\Delta 19}$ and Cx43-CT mutants: Cx43-$CT^{\Delta SH3}$, Cx43-$CT^{\Delta 19}$, $Cx43^{\Delta SH3\Delta 19}$ are indicated with colored lines

was sufficient to bind the CT and to inhibit the opening of Cx43-hemichannels, while not affecting Cx43 gap junctions [15, 16]. Thus, both TAT-L2 and Gap19 serve as novel and selective Cx43-hemichannel inhibitors and thus allow for the discovery of physiological functions of Cx43-hemichannels and for the therapeutic inhibition of excessive pathophysiological opening of Cx43-hemichannels, as observed under ischemic conditions in brain and heart [17].

Although the CT9 sequence was sufficient for restoring the activity of $Cx43^{M239}$-based hemichannels, deletion of the last 19 amino acids of the CT only had minor impact on its interaction with the L2 domain, indicating that other regions different from CT9 could contribute to loop/tail interaction. We here sought to identify other regions in the CT participating in loop/tail interactions to establish functionally active Cx43-hemichannels. In this study, we turned our focus on a previously identified 17-mer peptide, which

coincides with the SH3-binding domain that could interfere with the pH gating of Cx43 gap junctions [18]. Here, we identified the SH3-binding domain, in addition to the CT9 region, as a critical determinant for loop/tail interactions in Cx43-hemichannels, whereby (1) the SH3-binding domain applied as a synthetic peptide can overcome inhibition of Cx43-hemichannels by high $[Ca^{2+}]_i$ and restore the activity of CT-truncated $Cx43^{M242}$ hemichannels and (2) deletion of the SH3-binding domain in full-length Cx43-hemichannels abrogates Cx43-hemichannel activity. This study is the first to demonstrate that the SH3-binding domain, together with the last nine amino acids of the CT, is critical for Cx43-hemichannel activity.

Methods

Cell culture and transfections

Cultures of primary bovine corneal endothelial cells (BCECs) from fresh eyes were established as described previously [10, 19]. HeLa cells exogenously expressing full-length human Cx43, were established as a stable cell line [20]. HeLa cells (ATCC®) transiently expressing full-length Cx43 and CT-truncated mutants of Cx43 such as $Cx43^{\Delta 19}$, $Cx43^{\Delta SH3}$, $Cx43^{\Delta SH3\Delta 19}$ and $Cx43^{M242}$ were developed. All cells were cultured at 37 °C in a 5% CO_2 incubator.

Plasmid constructs

The pGEX-6p2 plasmid was used for the bacterial expression and purification of the Cx43-CT (full-length CT, aa 255-382) and of truncated Cx43-CT versions lacking the SH3-binding domain [(Cx43-$CT^{\Delta SH3}$) (aa SPTAPLSPMSPPG)], the last 19 amino acids (Cx43-$CT^{\Delta 19}$) or both the SH3-binding domain and the last 19 amino acids (Cx43-$CT^{\Delta SH3\Delta 19}$). The pcDNA3.1(−) plasmid was used for heterologous expression in HeLa cells of full-length Cx43, $Cx43^{\Delta SH3}$, $Cx43^{\Delta 19}$, $Cx43^{\Delta SH3\Delta 19}$ and $Cx43^{M242}$, which lacks the CT, and $Cx43^{\Delta Gap19M242}$, a CT-truncated Cx43 mutant that also lacks the Gap19 region. pGEX6p2-Cx43-CT and pGEX6p2-Cx43-$CT^{\Delta 19}$ were kindly provided by Prof. Mario Delmar (New York University School of Medicine, USA) and Paul L. Sorgen (University of Nebraska Medical Center, USA), while the pcDNA3.1(−)-$Cx43^{\Delta Gap19M242}$ plasmid was obtained from GenScript® (USA) via custom gene synthesis.

Peptides

All synthetic peptides (> 90% pure) (Table 1) were obtained from LifeTein (USA). TAT-peptides were used at 50 or 100 µM incubated with the cells for 30 min at 37 °C.

Antibodies

To detect the expression of Cx43 or CT-truncated variants using immunoblotting, the Cx43 antibody (N-term; Purified Rabbit Polyclonal Antibody; Abgent, USA) was used at a typical dilution of 1:2000. To detect the expression of $Cx43^{\Delta Gap19M242}$, the Cx43-E2 antibody (directed against the second extracellular loop; described in Siller-Jackson et al. [21]) was used at a dilution of 1:500. β-actin was used as a loading control, which was detected using an anti-β-actin antibody (Sigma) at a dilution of 1:15,000.

Imaging of intercellular Ca^{2+}-wave propagation

Intercellular Ca^{2+}-wave propagation was assayed as described previously [19, 22]. In brief, BCECs were loaded with Ca^{2+}-sensitive fluorescent dye Fluo-4 AM in PBS without Ca^{2+} and Mg^{2+} for 30 min at 37 °C. TAT-peptides (100 µM) were present in the bath solution during Fluo-4 AM loading. After washing the cells with PBS with Ca^{2+} and Mg^{2+}, the dye was excited at 488 nm, and its fluorescence emission was collected at 530 nm. Spatial changes in $[Ca^{2+}]_i$ following point mechanical stimulation (MS) were measured with the confocal microscope (LSM510, Zeiss) using a 40× objective (Air, 1.2 N.A.). A point MS, applied to a single cell, consisted of an acute deformation of the cell by briefly touching less than 1% of the surface area of

Table 1 Overview of the sequence of the different peptides used in this study

Name	Sequence
SH3	SPTAPLSPMSPPG
SH3 mutant	SATAVLSAMSVPG
TAT-SH3	YGRKKRRQRRRSSPTAPLSPMSPPG
TAT-SH3 mutant	YGRKKRRQRRRSSATAVLSAMSVPG
TAT-L2	YGRKKRRQRRRDGANVDMHLKQIEIKKFKYGIEEHGK
TAT-CT9	YGRKKRRQRRRSRPRPDDLEI
Biotin-L2	Biotin-DGANVDMHLKQIEIKKFKYGIEEHGK
Biotin-Gap19	Biotin-KQIEIKKFK

The TAT sequence is underlined. SH3 refers to the SH3-binding domain

its cell membrane with a glass micropipette (tip diameter < 1 µm) coupled to a piezoelectric crystal (Piezo device P-280, Amplifier-E463; PI Polytech, Karlsruhe, Germany) mounted on a micromanipulator, as described previously [10, 23]. Polygonal regions of interest (ROIs) were drawn to define the borders of each cell. Fluorescence was averaged over the area of each ROI. Normalized fluorescence (NF) was then obtained by dividing the fluorescence by the average fluorescence before MS. We quantified the propagation of the intercellular Ca^{2+} wave by measuring the total surface area of responsive cells (active area, AA) with NFP1.1, using imaging software (LSM Image 4.2; Zeiss).

Measurement of ATP release

ATP release from BCEC was measured via a luciferin–luciferase system [24]. One hundred microliter samples were taken from the 500 µl bathing solution covering the cells after exposure to mechanical stimulation and transferred to a custom-built photon counting set-up to measure the luminescence as described previously [23]. Briefly, photons emitted as a result of the oxidation of luciferin in the presence of ATP and O_2 and catalyzed by luciferase were detected by a photon counting photomultiplier tube (H7360-01; Hamamatsu Photonics, Hamamatsu, Japan). Voltage pulses from the photomultiplier module were counted with a high-speed counter (PCI-6602; National Instruments, Austin, Texas, USA). Dark count of the photomultiplier tube was < 80 counts/s. ATP release from HeLa cells, stably expressing full-length Cx43 or CT-truncated Cx43 ($Cx43^{M239}$) were triggered by A23187, a Ca^{2+} ionophore, and measured via a luciferin–luciferase system [25]. Cellular ATP release was accumulated over the period of trigger exposure (5 min). Baseline measurements were performed on separate cultures using standard HBSS-HEPES. ATP release from HeLa cells, transiently expressing Cx43, CT-truncated Cx43 ($Cx43^{M242}$) or deletion mutants of Cx43 ($Cx43^{\Delta 19}$, $Cx43^{\Delta SH3}$, $Cx43^{\Delta SH3\Delta 19}$ or $Cx43^{\Delta Gap19M242}$) were triggered by either EGTA or A23187. ATP release was normalized to the baseline signal. Results were obtained from at least four independent measurements.

Cell-surface biotinylation

The biotinylation experiment was performed as previously described [26]. Briefly, a monolayer of HeLa cells (~ 70% confluence) was cultured and was transfected with 5 µg of each plasmid (pcDNA empty vector, Cx43, $Cx43^{\Delta 19}$, $Cx43^{\Delta SH3}$ and $Cx43^{\Delta SH3\Delta 19}$). Next day, the cells were washed twice with ice-cold phosphate-buffered saline (PBS) and labeled with 0.25 mg/ml of sulfo-NHS-SS-biotin (Thermo Fisher Scientific) in PBS at 4 °C for 1 h without shaking. Biotinylation reaction was stopped by adding quenching solution. After 5 min, the solution was removed and washed with tris-buffered saline (TBS), which contains EDTA-free protease inhibitor (1 tablet per 50 ml of TBS buffer). Subsequently, the cells were scraped and lysed. The cell lysates (equal amounts) were incubated overnight with NeutrAvidin™ Agarose resin at 4 °C with end-over-end mixing. After this, the flow-through fractions were collected and beads were washed three times with washing buffer. Biotinylated proteins were eluted from beads using SDS-PAGE sample buffer contains DTT. Total lysate (10 µg) and equal amounts of flow-through and eluted fractions were analyzed by SDS-PAGE and subsequent immunoblotting. N-terminal Cx43 (Abgent) and β-actin (Sigma) antibodies were used for the Western blotting procedure.

Expression and purification of the Cx43-CT domain and deletion mutants

The GST-linked protein was expressed and purified from *E. coli* BL21(DE3) cells induced with 0.5 mM IPTG. The bacterial pellet was resuspended in cold lysis solution (20 mM Tris/HCl, pH 7.5, 500 mM NaCl, 1% Triton-X-100) containing protease inhibitors and cells were lysed by sonication. After removal of the cell debris by centrifugation, the soluble protein fraction was incubated with Glutathione Sepharose 4B for 2 h at 4 °C. The beads were collected and washed three times with PBS. The GST was removed using PreScission protease and dialyzed against 1X DPBS without $CaCl_2$ and $MgCl_2$ (Gibco®, Life Technologies) using 2-kDa MWCO dialyzing cassette (Slide-A-Lyzer®, Thermo Fisher Scientific). 30 KD, Amicon® Ultra Centrifugal Filter (Merck Millipore) was used to remove bacterial protein and collected filtrate as an analyte.

Surface plasmon resonance (SPR) experiments

SPR experiments were performed as described previously [15]. All binding experiments were performed using Biacore T200 instrument (GE Healthcare). The L2 and Gap19 peptide sequences were fused to biotin (Table 1). Equal amounts (resonance units or RU) of > 90% pure biotinylated peptides were immobilized on each flow cell of a streptavidin-coated sensor chip (Sensor Chip SA, Biacore Inc., Uppsala, Sweden) using HEPES buffer (in mM: 10 HEPES, 1 EDTA, 100 NaCl) with 0.005% polysorbate-20 (Tween-20) at pH 7.4. We used recombinant purified proteins such as Cx43-CT full-length, Cx43-$CT^{\Delta 19}$, Cx43-$CT^{\Delta SH3}$ and Cx43-$CT^{\Delta SH3\Delta 19}$ as an analyte using running buffer (in mM: 10 HEPES, 100 NaCl, pH 6.8) at a flow rate of 30 µl/min in random order (injection volume 120 µl). Bound protein was removed by injection of 10 µl regeneration buffer (50 mM NaOH, 1 M NaCl) at 10 µl/min. Background signals obtained from the

reference flow cell, containing the reversed biotinylated peptide, were subtracted to generate response curves.

Electrophysiological recording

Cx43-hemichannel currents were measured via whole-cell patch clamp recording as described by Bol et al. [27]. HeLa cells overexpressing Cx43 were bathed in a modified Krebs–Ringer solution consisting of (in mM): 150 NaCl, 6 CsCl, 2 $CaCl_2$, 2 $MgCl_2$, 1 $BaCl_2$, 2 pyruvate, 5 glucose, 5 HEPES and pH 7.4. The standard whole-cell recording pipette solution was composed of (in mM): 130 CsCl, 10 Na-aspartate, 0.26 $CaCl_2$, 1 $MgCl_2$, 2 EGTA, 5 tetraethyl ammonium (TEA)-Cl and 5 HEPES; pH was adjusted to 7.2. The Webmaxc Standard software (http://www.stanford.edu/~cpatton/webmaxcS.htm) was used to calculate the concentration of $CaCl_2$ needed to set the free [Ca^{2+}] in the pipette solution to 50 nM, 500 nM or 1 µM (three different solutions), respectively. Hemichannel currents were elicited by stepping the membrane potential from a holding potential of − 30 to + 60 mV (30 s) and recorded with an EPC 7 PLUS patch clamp amplifier (HEKA Elektronik, Lambrecht/Pfalz, Germany). Electrophysiological data were acquired at 4 kHz using a NI USB-6221 data acquisition device from National Instruments (Austin, TX, USA) controlled by the WinWCP acquisition software (developed by Dr. J. Dempster, University of Strathclyde, Glasgow) and filtered at 1 kHz (7-pole Bessel filter). Following holding current subtraction, charge transfer through open hemichannels (Q_m) was quantified by integrating unitary hemichannel activities over the duration of the applied voltage steps.

Statistical analysis

Data are represented as mean ± SEM. For statistical analyses, each treatment was compared to its respective control, and significance was determined using a one-way ANOVA or paired Student's *t* test, as appropriate, using GraphPad. In case of multiple comparisons, a Tukey's test was performed. Differences were considered significant at $P < 0.05$, indicated by the symbols *, $ or ^.

Results

Biotin-L2 and biotin-Gap19 interact with both Cx43-CT and Cx43-CT$^{\Delta 19}$

A schematic representation of the Cx43 protein with its four transmembrane domains and regions relevant for this study is presented in Fig. 1, including the L2 domain and its Gap19 subdomain within the CL as well as the SH3-binding domain (in figure panels and peptide nomenclature abbreviated as SH3) and CT9 region within the CT. The lines indicate the residues that were deleted in the Cx43-CT and full-length Cx43 constructs, resulting respectively in Cx43-CT$^{\Delta SH3}$, Cx43-CT$^{\Delta 19}$ and Cx43-CT$^{\Delta SH3\Delta 19}$ further applied in SPR studies and Cx43$^{\Delta SH3}$, Cx43$^{\Delta 19}$ and Cx43$^{\Delta SH3\Delta 19}$ used for exogenous expression in HeLa cells.

First, we applied the SPR assay to characterize the binding of the CT of Cx43 to the L2 and Gap19 loop domains of Cx43. The Cx43-CT and Cx43-CT$^{\Delta 19}$ proteins were expressed and purified as recombinant GST-fusion proteins from which the GST was removed via a PreScission protease. The different GST-Cx43CT-fusion proteins used in this study are schematically displayed in Fig. 2a. A total protein stain of an SDS-PAGE of the GST-cleaved proteins obtained after purification and used in the SPR experiments is shown in Fig. 2b. The L2 and Gap19 domain sequences were produced as synthetic peptides to which a biotin tag was added to their N terminus. Biotin-L2 and biotin-Gap19 and their scrambled counterparts were immobilized to a streptavidin-coated sensor chip. Similar amounts of the four peptides were loaded to the chip [i.e., approximately 800 resonance units (RU)]. The scrambled controls were used to monitor background binding, which was subtracted from all traces shown in this study. We used 5 µM of Cx43-CT and Cx43-CT$^{\Delta 19}$ to monitor their L2- and Gap19-binding characteristics. As observed before, we found that the CT of Cx43 could bind to L2 (Fig. 2c) and Gap19 (Fig. 2d). Strikingly, when comparing Cx43-CT and Cx43-CT$^{\Delta 19}$, binding to either L2 or Gap19 was decreased but not completely lost. This is remarkable, since the Cx43-CT$^{\Delta 19}$ protein does not harbor the CT9 region responsible for restoring Cx43^{M242}-hemichannel activity. This indicates that the Cx43-CT of Cx43 harbors another major binding site for the L2 and Gap19 domains.

Biotin-L2 and biotin-Gap19 fails to bind Cx43-CT$^{\Delta SH3\Delta 19}$

A study by the Delmar group [18] has shown that a 17-mer peptide covering amino acids 271-287 of Cx43 and corresponding to the SH3-binding domain, was proposed as the gating particle for Cx43 gap junction channels. Therefore, we asked whether the SH3-binding domain could be a target for L2 and Gap19. Cx43-CT$^{\Delta SH3}$ and Cx43-CT$^{\Delta SH3\Delta 19}$, developed and purified as GST-fusion proteins (Fig. 2a, b), were used as an analyte in their GST-clipped form in SPR experiments. Five µM of Cx43-CT$^{\Delta SH3}$ and CT$^{\Delta SH3\Delta 19}$ were exposed to biotinylated versions of L2 and Gap19 loop-located peptide sequences. Interestingly, Cx43-CT$^{\Delta SH3}$ displayed diminished binding to L2 and Gap19, whereas Cx43-CT$^{\Delta SH3\Delta 19}$ almost completely failed to bind to the two CL-derived peptides (Fig. 2c, d). These data designate the SH3-binding domain of the CT of Cx43 as a second and

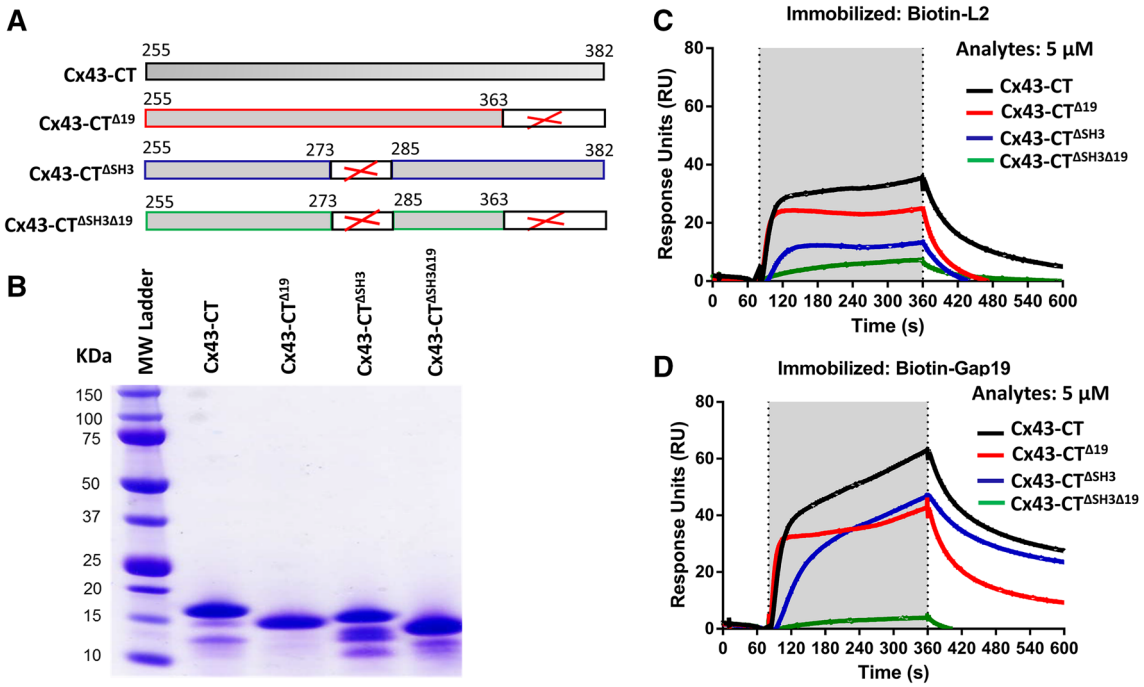

Fig. 2 The last 19 amino acids and the SH3-binding domain are two regions within the Cx43-CT that participate in interactions with the L2 or Gap19 region. **a** Schematic representation of the different Cx43-CT proteins used in this study. **b** GelCode Blue-stained SDS-PAGE gel showing the purified Cx43-CT, Cx43-CT$^{\Delta 19}$, Cx43-CT$^{\Delta SH3}$ and Cx43-CT$^{\Delta SH3\Delta 19}$ proteins after GST removal. 5 µg of protein was loaded per lane. **c**, **d** Sensorgrams obtained for Cx43-CT, Cx43-CT$^{\Delta 19}$, Cx43-CT$^{\Delta SH3}$ and Cx43-CT$^{\Delta SH3\Delta 19}$ applied as an analyte at 5 µM to streptavidin-coated sensor chips loaded with biotin-L2 (**c**) and biotin-Gap19 (**d**). In both cases, the presented resonance units (RU) signals were obtained by subtracting the non-specific binding of the proteins to biotin-L2 reverse. The application of the analyte is indicated by the gray region in the sensorgram

important target site for interaction with the L2 and Gap19 loop domains.

TAT-SH3 overcomes the inhibition of Cx43-hemichannels by conditions that activate the actomyosin-contractile system

We previously showed that mechanical stimulation of a monolayer BCECs elicits a Ca^{2+} rise in the mechanically stimulated cell that propagates to neighboring cells mainly via ATP released in the extracellular environment in a Cx43-hemichannel-dependent manner [10]. The propagation of the Ca^{2+}-wave to neighboring cells can be quantified as the active area, which is the total surface area of all cells within the monolayer that display an above-threshold $[Ca^{2+}]_i$ rise. We previously validated this approach showing that the active area was severely reduced by promoting extracellular ATP degradation [23], by knocking down Cx43 using siRNA and by pre-treating the cells with TAT-L2 that inhibits Cx43-hemichannels [10]. In previous work, we found that pre-treating BCECs with thrombin strongly reduced the active area due to an inhibition of Cx43-hemichannel activity [24]. The underlying mechanism was attributed to an activation of the actin-myosin cytoskeleton [24], since the inhibition of Cx43-hemichannels could be alleviated by (−)-blebbistatin [14]. We hypothesized that activation of the actin-myosin cytoskeleton resulted in loss of loop/tail interaction essential for Cx43-hemichannel activity, since TAT-CT9, a cell-permeable peptide containing the last nine amino acids of the Cx43 CT, could restore the thrombin-reduced active area and thus Cx43-hemichannel activity [10]. Here, we show that application of 100 µM TAT-SH3 peptide, a cell-permeable peptide containing the SH3-binding domain, alleviated the thrombin-induced inhibition of mechanical stimulation-induced Ca^{2+} waves and ATP release, indicating that TAT-SH3 peptide can alleviate the inhibition of Cx43-hemichannel by the contractile system (Fig. 3a, b). A TAT-SH3 mutant peptide (Pro274Ala, Pro277Val, Pro280Ala and Pro283Val mutants) was used as a negative control and was not able to overcome the effect of thrombin on the Ca^{2+}-wave propagation and ATP release. Figure 3a displays the normalized active area, calculated as the percentage of the untreated control condition, which was set at 100%. Figure 3b displays the normalized ATP release, calculated as the percentage of the untreated control condition (100%). This mechanism is also operative in cell models of HeLa, in which Cx43 is exogenously expressed. In these cells, A23187 can be applied at different concentrations to induce

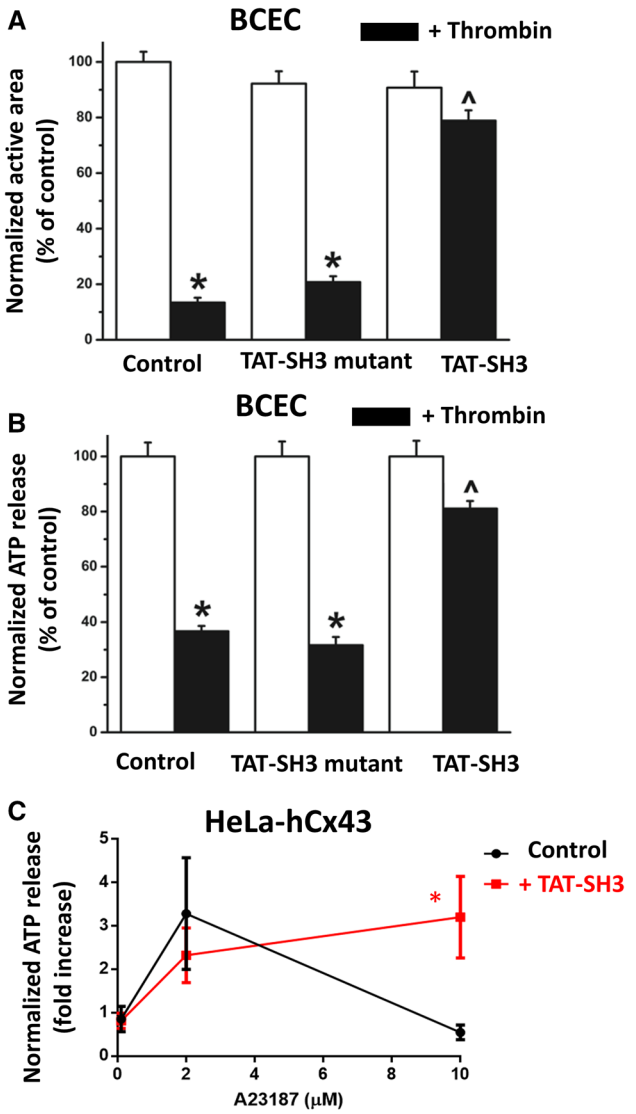

Fig. 3 TAT-SH3 peptide overcomes the inhibition of endogenous Cx43-hemichannels by contractility in primary BCECs. **a**, **b** Quantification of the active area of intercellular Ca^{2+} waves in BCECs (**a**) and ATP release from BCECs (**b**) provoked by mechanical stimulation in control or thrombin-treated conditions ($n = 3$). The effect of TAT-SH3 or TAT-SH3 mutant peptides (100 μM) on the active area (**a**) and the ATP release (**b**) was determined for control and thrombin-treated conditions. Asterisk indicates a significant difference from the untreated condition, while caret symbol indicates a significant difference from the thrombin-treated control. **c** Quantification of the ATP release from HeLa cells exogenously expressing Cx43 exposed to [A23187] (0.1, 2 and 10 μM) in the absence or presence of TAT-SH3 (100 μM). Data display ATP release as fold induction of baseline values ($n = 5$). Asterisk indicates a significant difference between the control and TAT-SH3-treated condition

a $[Ca^{2+}]_i$ elevation to ~ 500 nM (using 2 μM A23187) as a "Cx43-hemichannel-activating condition" and to approximately 1 μM (using 10 μM A23187) as a "Cx43-hemichannel-inhibiting condition" as previously described [10, 25]. This results in a typical convex-up bell-shaped dependence of Cx43-hemichannel activity towards $[Ca^{2+}]_i$, which was previously determined in detail using a range of different concentrations of A23187 [12]. Importantly, similar to the data obtained in BCECs (Fig. 3a, b), Cx43-hemichannel activity from HeLa cells exogenously expressing Cx43 could be modulated by TAT-SH3 (100 μM), whereby the high $[Ca^{2+}]_i$-induced inhibition of Cx43-hemichannel-mediated ATP release was alleviated by TAT-SH3 (Fig. 3c).

SH3 peptide alleviates the high $[Ca^{2+}]_i$-induced inhibition of Cx43-hemichannel single channel activity in whole-cell patch clamp recording

To assess the effect of the SH3-binding domain peptide on Cx43-hemichannels at the single channel level, whole-cell patch clamp recordings of HeLa cells exogenously expressing Cx43-hemichannels were performed (Fig. 4). The SH3-binding domain and mutant SH3-binding domain peptides (100 μM) were delivered to the cells via the patch pipette. We also used the CT9 peptide (100 μM) as a positive control. Voltage steps from a holding potential of − 30 to + 60 mV at different $[Ca^{2+}]_i$ were applied to elicit Cx43-hemichannel activity.

Consistent with previous observations, Cx43-hemichannels displayed a bell-shaped dependence towards $[Ca^{2+}]_i$. At 50 nM $[Ca^{2+}]_i$, the voltage steps triggered limited hemichannel-opening activity that was strongly increased when $[Ca^{2+}]_i$ was set to 500 nM (Fig. 4a, d). Figure 4e demonstrates that the recorded single channel activities were all in the 220 pS range, typical for Cx43-hemichannels. Further increasing $[Ca^{2+}]_i$ to 1 μM resulted in the disappearance of hemichannel activity as depicted in Fig. 4f. Figure 4j summarizes average data of the total membrane charge transfer (Q_m) associated with unitary current activity, obtained by integrating the current over time, demonstrating low hemichannel activity at 50 nM $[Ca^{2+}]_i$, increased hemichannel opening activity at 500 nM $[Ca^{2+}]_i$ and disappearance of the activity at 1 μM $[Ca^{2+}]_i$. The bell-shaped dependence of Cx43-hemichannels towards $[Ca^{2+}]_i$ can be appreciated from the experiments without peptides, indicated in red bars in Fig. 4j.

Application of either the SH3 peptide (Fig. 4b) or the CT9 peptide (Fig. 4c) at 50 nM $[Ca^{2+}]_i$ did not affect the hemichannel opening activity. However, delivering the SH3-binding domain peptide to the cells completely prevented the inhibition of Cx43-hemichannel currents by 1 μM $[Ca^{2+}]_i$ (Fig. 4g); by contrast, the mutant SH3-binding domain peptide failed to do this (Fig. 4h). The CT9 peptide, applied as a positive control condition, also prevented the disappearance Cx43-hemichannel activity at 1 μM $[Ca^{2+}]_i$ (Fig. 4i). The Q_m summary data indicated that hemichannel activities rescued by the SH3 peptide at high $[Ca^{2+}]_i$ (1 μM) were similar to those observed by application of the CT9 peptide (100 μM)

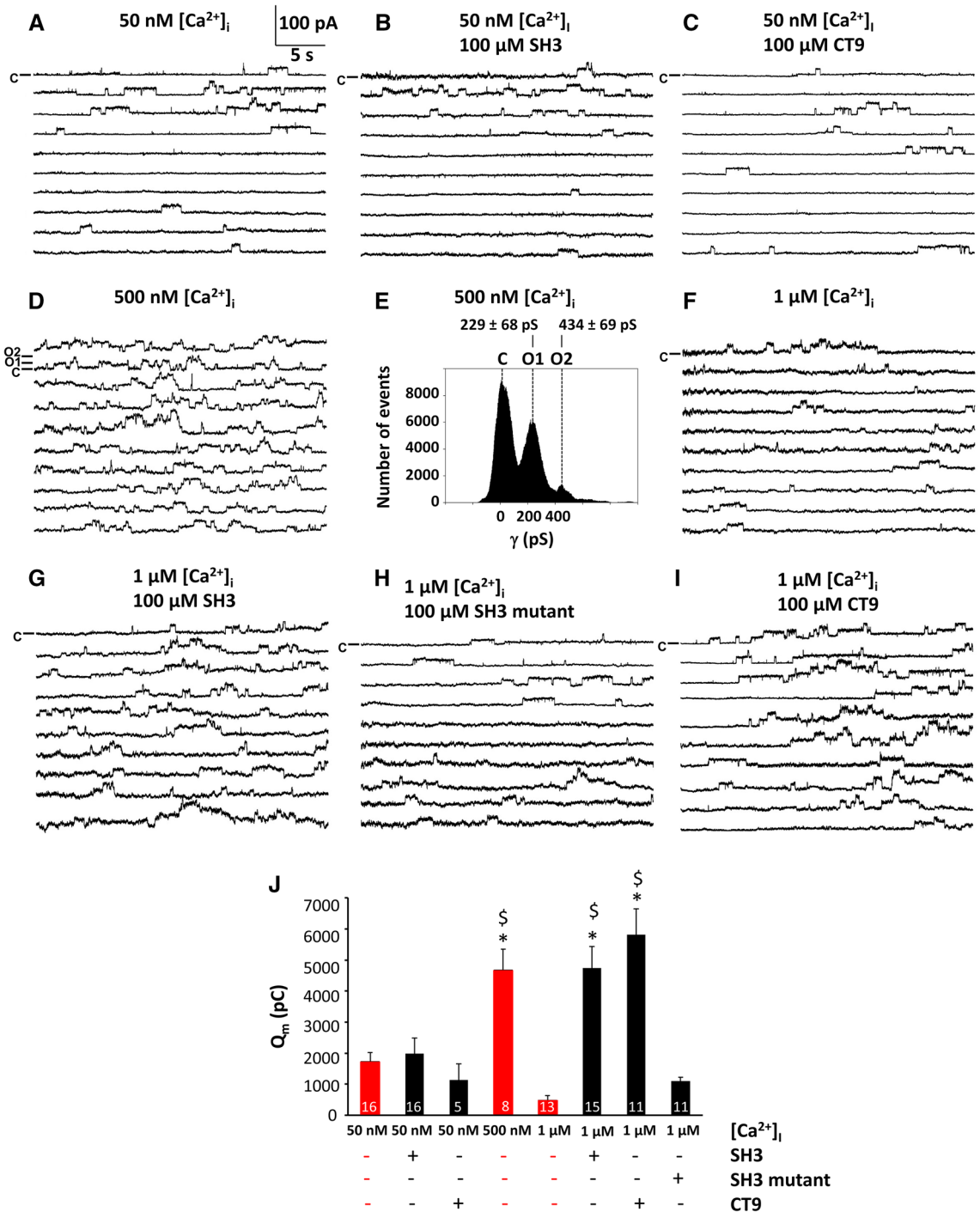

and to the Cx43-hemichannel activity triggered by 500 nM $[Ca^{2+}]_i$ (Fig. 4j).

As an additional control, we independently verified whether the observed currents induced by the SH3-binding domain and CT9 peptides were originating from Cx43-hemichannels. For this, we performed experiments on native HeLa cells, which lack endogenous Cx43 expression (Supplementary Fig. 1). In these experiments, voltage steps from − 30 to + 60 mV did not trigger any unitary current activity and application of either the SH3-binding domain or the CT9 region as peptides (100 µM) at 1 µM $[Ca^{2+}]_i$ did not elicit any changes.

These electrophysiological data obtained at the single channel level further underpin the critical role of the SH3-binding domain in maintaining Cx43-hemichannel activity in conditions of high $[Ca^{2+}]_i$.

◂**Fig. 4** SH3 and CT9 peptide overcome the inhibition of the activity of single Cx43-hemichannels. Panels **a**–**i** (except panel **e**) display example traces of unitary currents obtained by 30 s voltage steps from − 30 to + 60 mV in Cx43-overexpressing HeLa cells, whereby the closed state is indicated on the first trace with the symbol C. In panel **d**, open state 1 (O1) indicates a single channel opening event and open state 2 (O2) the opening of another channel superimposed on the first one. The $[Ca^{2+}]_i$ conditions indicated were applied via the whole-cell recording pipette. Peptides were added at 100 µM final concentrations. **a**–**c** Example traces showing unitary currents obtained at 50 nM $[Ca^{2+}]_i$, which corresponds to resting $[Ca^{2+}]_i$ conditions, in the absence (**a**) or presence of peptides, namely SH3-binding domain (**b**) and CT9 region (**c**). **d** Example traces showing unitary currents obtained at 500 nM $[Ca^{2+}]_i$, which corresponds to the range of $[Ca^{2+}]_i$ rises occurring upon physiological signaling. **e** All-point histogram obtained from the recordings depicted in **d**, indicating a single channel conductance in the ~ 220 pS range. **f**–**i** Example traces showing unitary currents obtained at 1 µM $[Ca^{2+}]_i$, which corresponds to a $[Ca^{2+}]_i$ that is able to activate the actomyosin cytoskeleton, in the absence (**f**) or presence of peptides, namely SH3-binding domain (**g**), a mutant of the SH3-binding domain (**h**) and the CT9 region (**i**). **j** Summary data obtained by integrating the current traces over time, giving the membrane charge transfer (Q_m), for the different conditions applied. The bar graph illustrates that SH3 and CT9 peptides remove hemichannel inhibition at 1 µM $[Ca^{2+}]_i$ while mutant SH3 is inactive. Bars corresponding to control conditions without peptide additions are shown in red. Asterisk and dollar sign indicate significant difference compared to the condition with $[Ca^{2+}]_i$ being 50 nM and 1 µM, respectively

$Cx43^{\Delta SH3\Delta 19}$ fails to release ATP in response to moderate $[Ca^{2+}]_i$ rises or buffering $[Ca^{2+}]_e$

Armed with our knowledge that TAT-SH3 could also restore the activity of transiently expressed Cx43 variants, we wondered whether the activity of full-length Cx43-hemichannels were critically dependent on the presence of the last 19 amino acids and/or the SH3-binding domain. In other words, we asked whether the loss of function of CT-truncated Cx43 could be replicated by deletion of either one of these regions or the combined deletion of these regions. We generated $Cx43^{\Delta 19}$, $Cx43^{\Delta SH3}$ and $Cx43^{\Delta SH3\Delta 19}$ constructs for transient expression in HeLa cells. Using immunoblotting with an antibody having its epitope in the N-terminal part of the protein, we show that Cx43, $Cx43^{\Delta 19}$, $Cx43^{\Delta SH3}$ and $Cx43^{\Delta SH3\Delta 19}$ are properly expressed in HeLa cells, establishing conditions at which all four proteins were expressed at similar levels (Fig. 5a). We show that both lowering $[Ca^{2+}]_e$ (by addition of 5 mM EGTA), a well-known hemichannel opening condition, or moderately increasing $[Ca^{2+}]_i$ (2 µM A23187) resulted in increased ATP release that was significantly above the response in non-transfected cells, indicating ATP release resulted from hemichannel activity. Interestingly, $Cx43^{\Delta 19}$ and $Cx43^{\Delta SH3}$ displayed a strongly reduced hemichannel activity, although some remnant ATP release could be observed. $Cx43^{\Delta SH3\Delta 19}$ displayed a complete loss of the ATP release attributed to Cx43-hemichannels, indicating that deletion of both regions completely abrogate hemichannel activity (Fig. 5b). These data indicate that both the SH3-binding domain and the last 19 amino acids of the Cx43-CT are required for proper Cx43-hemichannel function. Next, we aimed to exclude that the loss of hemichannel activity observed for the deletion mutants was due to their inability to traffic to the plasma membrane. Therefore, we performed surface biotinylation experiments on Cx43 and its deletion mutants. Via this approach, surface accessible proteins are biotinylated and captured. As an internal control, we used β-actin, an intracellular protein. This approach shows that Cx43, $Cx43^{\Delta 19}$, $Cx43^{\Delta SH3}$ and $Cx43^{\Delta SH3\Delta 19}$ all reached the cell surface to a comparable degree (Fig. 5c).

TAT-SH3 restores the activity of CT-truncated $Cx43^{M242}$ hemichannels

We previously have demonstrated that loop/tail interactions are essential for the opening of Cx43-hemichannels [10]. Indeed, in contrast to full-length Cx43-based hemichannels, $Cx43^{M242}$-based hemichannels, which lack a large part of the CT, could not be opened by increases in $[Ca^{2+}]_i$. Therefore, we wondered whether TAT-SH3 was able to restore the activity $Cx43^{M242}$-based hemichannels. We used the TAT-CT9 peptide as a positive control, which was previously shown to restore the hemichannel activity of CT-truncated Cx43-hemichannels [10]. $Cx43^{M242}$ was transiently expressed in HeLa cells (Fig. 6a) and $Cx43^{M242}$-hemichannel activity was assessed by ATP release in response to 2 µM A23187 exposure. TAT-SH3 (100 µM) restored the ATP release properties of $Cx43^{M242}$ hemichannels, but mutant TAT-SH3 peptide failed to do this (Fig. 6b). Thus, similar to TAT-CT9, TAT-SH3 can restore the activity of CT-truncated Cx43-based hemichannels.

We also assessed the combination of TAT-SH3 and TAT-CT9 at different concentrations. At 50 µM both peptides added separately remained able to restore the ATP release of $Cx43^{M242}$ hemichannels in response to EGTA (5 mM), but the potency of these responses was less than when applied at 100 µM (Fig. 6c). Importantly, when combining 50 µM TAT-SH3 and 50 µM TAT-CT9, the ATP release activity of $Cx43^{M242}$ hemichannels was significantly higher compared to the ATP release activity induced by 50 µM TAT-SH3 or 50 µM TAT-CT9 applied separately and very similar to the activities observed by 100 µM TAT-SH3 or 100 µM TAT-CT9. Moreover, the combination of 100 µM TAT-SH3 and 100 µM TAT-CT9 did not induce a higher effect than 100 µM TAT-SH3 or 100 µM TAT-CT9 alone, likely indicating that the peptides when applied at 100 µM occupy all binding sites and thus elicit a maximal effect (Fig. 6d). Finally, to further underpin that the increased ATP release observed by TAT-SH3 and TAT-CT9 was dependent on the presence of $Cx43^{M242}$, empty vector-transfected HeLa cells did not display an increase in EGTA-induced ATP release

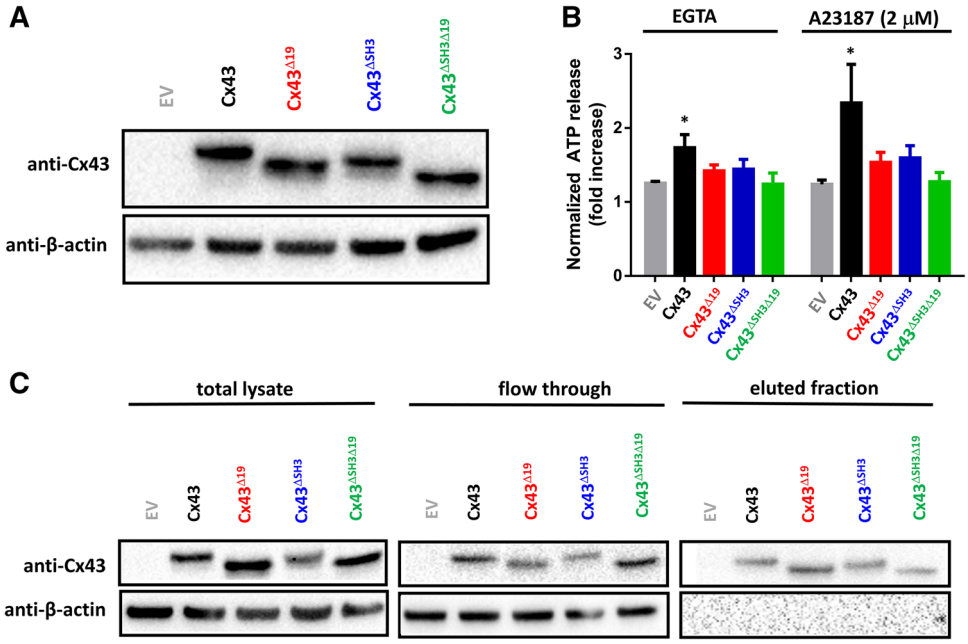

Fig. 5 Cx43 requires the last 19 amino acids and the SH3-binding domain to enable hemichannel activity. **a** An immunoblot stained with anti-Cx43 (N-term) (upper blot) or anti-β-actin (lower blot) for lysates (10 µg of lysate/lane) obtained from HeLa cells transfected with empty vector (EV), Cx43, Cx43$^{\Delta 19}$, Cx43$^{\Delta SH3}$ and Cx43$^{\Delta SH3\Delta 19}$ [pcDNA3.1-(−) plasmids]. **b** ATP release in response to EGTA or A23187 (2 µM) through hemichannels established by Cx43, Cx43$^{\Delta 19}$, Cx43$^{\Delta SH3}$ and Cx43$^{\Delta SH3\Delta 19}$, transiently expressed in HeLa cells; empty vector was used as a control. ATP release is shown as fold increase compared to baseline values ($n = 5$). **c** Cell-surface biotinylation and subsequent streptavidin purification experiment performed on HeLa cells expressing empty vector, Cx43, Cx43$^{\Delta 19}$, Cx43$^{\Delta SH3}$ and Cx43$^{\Delta SH3\Delta 19}$. The upper blots show Cx43 (anti-Cx43 N-term) and the lower blots show actin (anti-β-actin), an intracellular protein that serves on the one hand as a loading control and on the other hand as a negative control for the experiment. On the left, blots containing total lysates are displayed. In the middle, blots containing the flow-through fraction, which is the fraction that is not biotinylated (i.e., fraction that is not present on the surface). On the right, blots containing the eluted fraction are displayed, which is the biotinylated fraction (i.e., fraction that is present on the surface). Cx43 and the different Cx43-deletion variants appear in the surface-exposed fraction, while actin, an intracellular protein, is not, showing the validity of this approach

upon application of TAT-SH3 or TAT-CT9 (Supplementary Fig. 2). Thus, these data indicate that the SH3-binding domain can cooperate with the CT9 region to restore the activity of Cx43^{M242} hemichannels, which is in full agreement with the functional data obtained for Cx43$^{\Delta SH3\Delta 19}$ hemichannels.

TAT-SH3 fails to restore the activity of Cx43$^{\Delta Gap19M242}$

Next, we tested whether the effect of TAT-SH3 on Cx43^{M242} was dependent on the interaction with cytoplasmic loop region and more particularly the Gap19/L2 domains. Therefore, we applied two strategies, one based on competitive inhibition using the TAT-L2 peptide and one based on deleting the Gap19 region in Cx43^{M242}. For the first approach, we co-applied TAT-SH3 together with TAT-L2. We hypothesized that TAT-L2 by binding the SH3-binding domain peptide may act as a sink for TAT-SH3, reducing the amount of "free" TAT-SH3 available for Cx43^{M242} hemichannels. As such, TAT-L2 may compete with Cx43^{M242} for binding the TAT-SH3 peptide. In support of this hypothesis, the effect of TAT-SH3 on Cx43^{M242}-hemichannels could be neutralized by co-application of TAT-L2 peptide (Fig. 7a). For the second approach, we developed Cx43^{M242} hemichannels that lack the Gap19 domain (Cx43$^{\Delta Gap19M242}$). In contrast to activity of Cx43^{M242}, the ATP release through Cx43$^{\Delta Gap19M242}$-based hemichannels in response to 2 µM A23187 could not be restored by TAT-SH3 (Fig. 7a). We validated that the lack of effect of TAT-SH3 on Cx43$^{\Delta Gap19M242}$ was not due to a defective expression of this protein. Indeed, the expression of Cx43$^{\Delta Gap19M242}$ in HeLa cells could be confirmed using an antibody directed against the second extracellular loop (anti-Cx43-E2) (Fig. 7b). Hence, these data indicate that the SH3-binding domain can restore the activity of Cx43^{M242} channels by targeting the Gap19 sequence within the L2 region. These data correlate with our molecular interaction studies showing that the L2 region and more particularly the Gap19 region is a target of the SH3-binding domain. Thus, the lack of activity of Cx43^{M242}-based hemichannels is in part due to a loss of loop/tail interaction involving the SH3-binding domain and the Gap19 region.

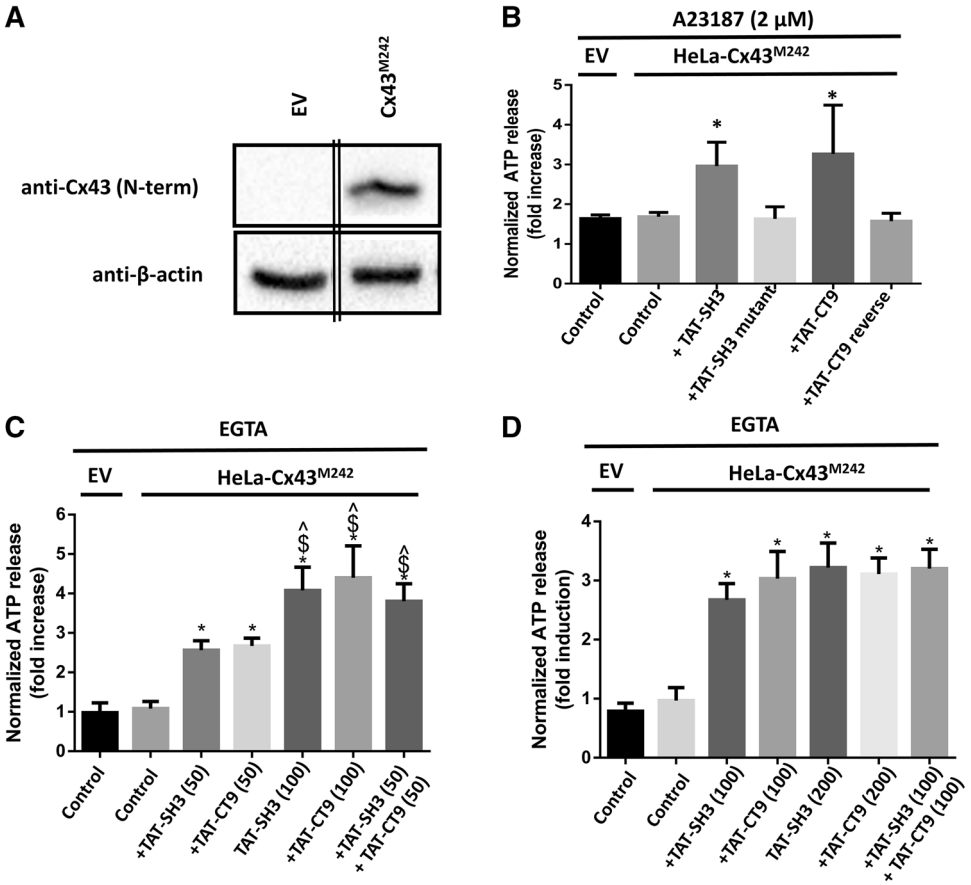

Fig. 6 The activity of CT-truncated Cx43-hemichannels can be restored by TAT-SH3 peptide. **a** An immunoblot stained with anti-Cx43 (N-term) (upper blot) or anti-β-actin (lower blot) for lysates (10 μg of lysate/lane) obtained from HeLa cells transfected with empty vector (EV) and $Cx43^{M242}$ (10 μg of lysate/lane). The double lines indicate that the lanes originating from the same gel/blot and exposure time were merged together. **b** HeLa cells transiently expressing EV or $Cx43^{M242}$ were exposed to 2 μM A23187. ATP release was determined in the presence of vehicle (control), TAT-SH3, TAT-SH3 mutant, TAT-CT9 and TAT-CT9 reverse peptides, all provided at 100 μM. **c** Similar experiment as in B, but cells were exposed to 50 μM TAT-SH3, 50 μM TAT-CT9, 100 μM TAT-SH3, 100 μM CT9 or 50 μM TAT-SH3 + 50 μM TAT-CT9. Asterisk indicates significantly different from EV control; caret symbol indicates significantly different from 50 μM SH3; dollar sign indicates significantly different from 50 μM CT9. **d** Similar experiment as in **b**, but cells were exposed to 100 μM TAT-SH3, 100 μM TAT-CT9, 200 μM TAT-SH3 or 200 μM CT9, or 100 μM TAT-SH3 + 100 μM TAT-CT9. Asterisk indicates significantly different from EV control. **b–d** In all ATP release experiments displayed, empty vector-transfected HeLa cells were used to determine the background ATP release in the absence of exogenous Cx43 (EV control). Control indicates that the cells were only treated with A23187 or EGTA and vehicle but not with peptide. Data show normalized ATP release as fold induction of baseline values before the stimulus (A23187 or EGTA) and were obtained from 3 to 6 independent experiments

Discussion

The major findings of this work are (1) that the CL is targeted by the SH3-binding domain located in the CT of Cx43 and (2) that the SH3-binding domain, together with the CT9 region, is important for Cx43-hemichannel opening in response to activating stimuli-like moderate rises in $[Ca^{2+}]_i$ rises or lowering of $[Ca^{2+}]_e$. Thus, besides the CT9 region, SH3-binding domain also contributes to the interaction of the Cx43-CT with the L2/Gap19 region on the CL, thereby controlling hemichannel opening (see Fig. 8 for a model). The SH3-binding domain delivered to cells as a TAT-fused peptide could alleviate the inhibition of Cx43-hemichannel activity by high $[Ca^{2+}]_i$/enhanced contractility and restored hemichannel activity of CT-truncated Cx43 variants. Moreover, deleting the SH3-binding domain as well as deleting the last 19 amino acids in full-length Cx43 impaired hemichannel activity, consistent with the fact that both regions harbor an L2/Gap19-binding site. Indeed, co-deletion of the last 19 amino acids and the SH3-binding domain completely abrogated Cx43-hemichannel activity. Finally, TAT-SH3 could restore the activity of CT-truncated Cx43-hemichannels, but this effect of TAT-SH3 critically depended on the presence of the Gap19 domain within the CL. Also, using submaximal concentrations of TAT-SH3 and TAT-CT9, we demonstrated that TAT-SH3 and TAT-CT9 can cooperate

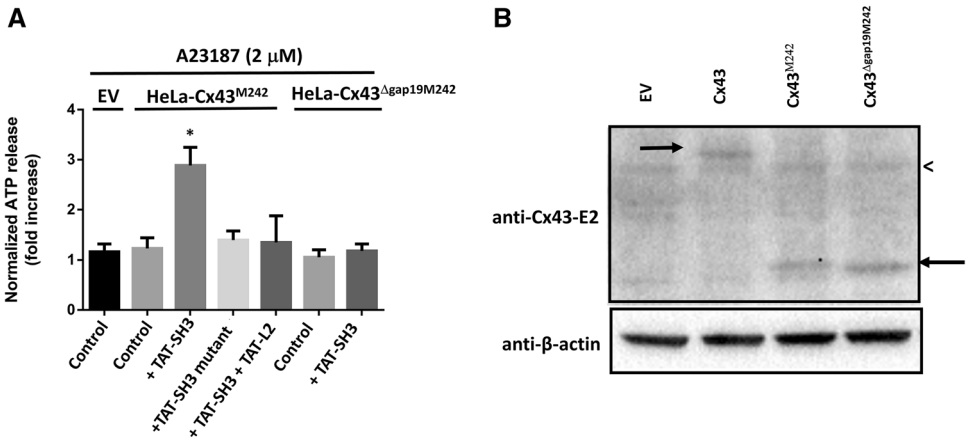

Fig. 7 TAT-SH3 fails to restore the activity of $Cx43^{\Delta Gap19M242}$. **a** HeLa cells transiently expressing EV, $Cx43^{M242}$ or $Cx43^{\Delta Gap19M242}$ were exposed to 2 μM A23187. ATP release was determined in the presence of vehicle (control), TAT-SH3, TAT-SH3 mutant and TAT-SH3 + TAT-L2, all provided at 100 μM. We used empty vector-transfected HeLa cells to determine the background ATP release in the absence of exogenous Cx43. Control indicates that the cells were only treated with A23187 and vehicle but not with peptide. Data show ATP release as fold induction of baseline values ($n = 4$). **b** An immunoblot stained with anti-Cx43 (E2) (upper blot) or anti-β-actin (lower blot) for lysates (30 μg of lysate/lane) obtained from HeLa cells transfected with empty vector (EV), Cx43, $Cx43^{M242}$ and expression of $Cx43^{\Delta Gap19M242}$. The left arrow indicates Cx43, while the right arrow indicates $Cx43^{M242}$ and $Cx43^{\Delta Gap19M242}$. The less than sign indicates a non-specific band also present in lysates obtained from empty vector-transfected HeLa cells (HeLa-EV)

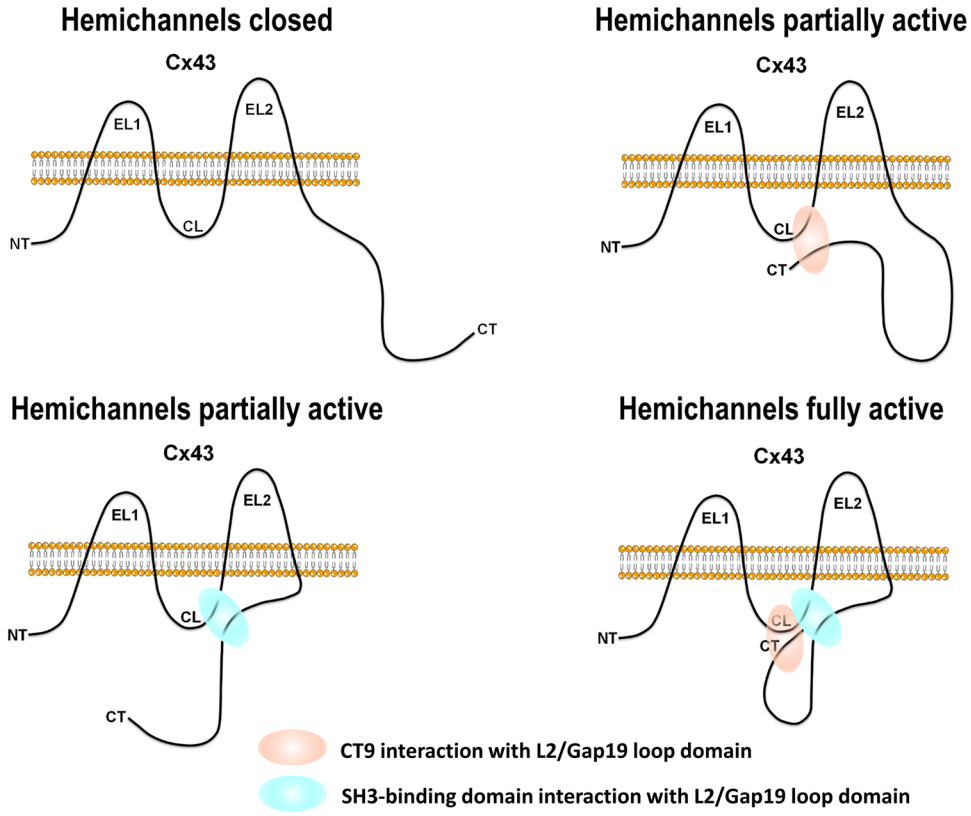

Fig. 8 Model for the regulation of Cx43-hemichannels by the two different CT regions. The panels represent one subunit of a hexameric Cx43-hemichannel. Two regions within the CT of Cx43 are important to establish fully active hemichannels in response to channel-opening triggers such as lowering $[Ca^{2+}]_e$ or moderately elevating $[Ca^{2+}]_i$. Cx43-hemichannels that cannot establish CT/CL interactions, e.g., by lacking the CT9 region and the SH3-binding domain (upper left), remain closed. Cx43-hemichannels that can only establish CT/CL interactions with one of the two domains, e.g., by lacking the SH3-binding domain (upper right) or the CT9 region (lower left), are partially active. Cx43-hemichannels that can engage both the CT9 region and the SH3-binding domain to interact with the CL are fully active (lower right)

to restore the activity of CT-truncated Cx43-hemichannels. Thus, our data indicate that two regions within the C-terminal tail of Cx43 are important for establishing loop/tail interaction that are needed for proper Cx43-hemichannel opening, namely the SH3-binding domain and the last nine amino acids. However, further work will be needed to unravel the exact interplay between the SH3-binding domain and the CT9 region for controlling the activity of full-length

Cx43-hemichannels. For instance, it is not clear whether in full-length Cx43 the SH3-binding domain and CT9 domain may compete for the Gap19 region within the CL or whether they may act in a concerted action thereby co-targeting the gap19 region, potentially by targeting different residues within this region. Furthermore, it is known that several regions within the CT are also involved in dimerization of the CT, which may contribute to the functional impact of these regions in Cx43-hemichannels, as detailed below.

Seminal work of the Delmar team indicated that Cx43 gap junctions are critically controlled by loop/tail interactions via a ball-and-chain model [6, 28, 29]. Under normal (healthy) conditions, Cx43 gap junctions are open (this does not mean that all channels in a gap junction are open [30]). Under ischemic conditions or acidification, Cx43 gap junctions close due to an interaction of the loop with the tail, according to a particle receptor model. This impairs the junctional coupling between cells, as occurs in cardiomyocytes in cardiac ischemia. Cx43 gap junction closure can be prevented by providing cells with a peptide mimicking the second part of the intracellular loop of Cx43, more specifically the L2 domain, which is the target of the Cx43-CT and prevents CT binding to the endogenous L2 region that acts to close gap junction channels [31].

Strikingly, conditions that close Cx43 gap junctions appear to trigger Cx43-hemichannel opening, such as metabolic inhibition of cortical astrocytes [5] or exposure of astrocytes to inflammatory cytokines [32] or ischemia-reperfusion in brain [33] and heart [10]. Hence, the mechanism accounting for this was proposed to relate to loop/tail interactions exerting opposite effects on Cx43 gap junctions as compared to Cx43-hemichannels [10]. Indeed, while interaction of the L2 region with the CT favors Cx43-hemichannel opening, it provokes Cx43 gap junction channel closure [10]. This could be attributed to a direct binding of the L2 region to the last nine amino acids of the Cx43 protein. In line with this, the Cx43-inhibitory properties of L2 could be reversed by co-addition of the CT9 region. Moreover, Cx43-hemichannels display a bell-shaped dependence on $[Ca^{2+}]_i$, where moderate $[Ca^{2+}]_i$ increases result in Cx43-hemichannel opening while high $[Ca^{2+}]_i$ increases result in Cx43-hemichannel closure [11, 12, 15, 27]. The inhibitory phase of this curve appeared to be due to activation of the actin/myosin cytoskeleton, since (−)-blebbistatin, an inhibitor of myosin-ATPase activity, could overcome the loss of Cx43-hemichannel activity brought about by high $[Ca^{2+}]_i$ [4]. Importantly, similar to (−)-blebbistatin, TAT-CT9 peptides could overcome the inhibition of Cx43-hemichannels by high $[Ca^{2+}]_i$, suggesting that high $[Ca^{2+}]_i$ results in activation of the actin-myosin cytoskeleton that prevents loop/tail interaction necessary for Cx43-hemichannel activity. Moreover, CT-truncated Cx43-hemichannels were inactive, but their activity could be restored by just providing the last nine amino acids as a TAT-CT9 peptide.

Here, we show that the SH3-binding domain is able to prevent Cx43-hemichannel inhibition by high $[Ca^{2+}]_i$ and restore the activity of CT-truncated Cx43-hemichannels. We propose that the SH3-binding domain can exert this function by establishing an interaction with the L2/Gap19 region. This is supported by two lines of evidence: (1) deletion of the SH3-binding domain in Cx43-CT strongly impairs its interaction with biotin-L2 (or Gap19 region) and (2) the restoration of hemichannel activity of CT-truncated Cx43 by the SH3-binding domain delivered as a peptide can be antagonized by the L2 peptide. These findings are in line with those of Duffy et al. [28], which confirmed interaction of a peptide covering the SH3-binding domain with the L2 sequence [28]. A challenging aspect to this model is that residues identified by NMR in the Cx43-CT to interact with the intracellular loop were mainly located in regions between aa 340 and 348 (an α-helical domain) and between aa 364–382 (the CT9 domain) [34]. Deletion of these regions impaired, but not completely abolished the binding between the CT and the CL in SPR experiments, indicating that other regions may participate in loop/tail interactions. Alternatively, deletion of the SH3-binding domain may affect the overall structure of the Cx43-CT, thereby indirectly impairing the interaction between L2 (or Gap19) and the Cx43-CT. Such indirect effect has been described by Sorgen et al. [35], whereby c-Src interacts with the SH3 domain on the Cx43 CT and thereby displaces the ZO-1–CT interaction which is located ~ 100 amino acids away from the SH3 domain [35]. Although an indirect effect of the SH3-binding domain on the Cx43-CT structure may explain the ability of TAT-SH3 to overcome the inhibition of Cx43-hemichannels by high $[Ca^{2+}]_i$, this model could definitely not account for the ability of TAT-SH3 to restore the activity of Cx43-hemichannels that lack most of the CT. This observation also precludes that the effect of TAT-SH3 on Cx43-hemichannels is mediated by changes in CT dimerization and/or by interference with associated proteins that target the SH3-binding domain, such as c-Src. Moreover, a study by Gangoso and co-workers [36] focusing on the regulation of Cx43 gap junctions by c-Src in the context of glioma stem cells indicated that in contrast to longer peptide variants (aa 245–283 and aa 266–283), the peptide corresponding to the minimal SH3-binding domain (aa 274–283) and closely resembling the peptide used in our study, did not affect the activity of c-Src. Therefore, in follow-up work, it will be interesting to assess the impact of these longer peptides on Cx43-hemichannel activity to delineate the contribution of c-Src inhibition and/or c-Src dissociation. Finally, another intriguing finding is that the SH3-binding domain affects Cx43-CT residues that participate in interactions with the PDZ2 domain, thereby

being able to partially impair the Cx43-CT/PDZ2 complex [35].

In conclusion, we show that the SH3-binding domain participates in establishing loop/tail interactions in Cx43-hemichannels and controlling Cx43-hemichannel activity.

Acknowledgements The authors are grateful to Anja Florizoone, Marina Crabbe, Tomas Luyten and Kirsten Welkenhuyzen for technical support. This work was supported by research Grant (G.0298.11 to GB and LL) and krediet aan navorsers (15117.14 N to CDH and GB) from the Research Foundation–Flanders (FWO) and by NIH grant CA196214 and Welch Foundation grant AQ-1507 (to JXJ). GB and LL are part of a Scientific Research Community supported by the FWO. The authors are thankful to Raf Ponsaerts and Elke De Vuyst for preliminary work and previous support and to Joris Vriens for helpful suggestion for displaying the electrophysiological recordings. The authors are also grateful to Mario A Delmar (New York University School of Medicine, NY, USA) and Paul L Sorgen (University of Nebraska Medical Center, NE, USA) for providing Cx43-expression plasmids.

Author contributions GB and LL conceived the study, supervised the work and interpreted data. JI, NW and CDH performed experiments and analyzed data. JJX provided critical reagents. JI performed cloning, protein purifications, SPR experiments, ATP release assays. CDH performed Ca^{2+}-wave propagations. NW performed all electrophysiology experiments. GB drafted the manuscript with further input and corrections by LL, JI, NW and CDH. All authors have read and approved the manuscript.

References

1. Kar R et al (2012) Biological role of connexin intercellular channels and hemichannels. Arch Biochem Biophys 524(1):2–15
2. Retamal MA, Saez JC (2014) Hemichannels; from the molecule to the function. Front Physiol 5:411
3. Iyyathurai J et al (2013) Peptides and peptide-derived molecules targeting the intracellular domains of Cx43: gap junctions versus hemichannels. Neuropharmacology 75:491–505
4. Ponsaerts R et al (2012) The contractile system as a negative regulator of the connexin 43 hemichannel. Biol Cell 104(7):367–377
5. Contreras JE et al (2002) Metabolic inhibition induces opening of unapposed connexin 43 gap junction hemichannels and reduces gap junctional communication in cortical astrocytes in culture. Proc Natl Acad Sci USA 99(1):495–500
6. Morley GE, Taffet SM, Delmar M (1996) Intramolecular interactions mediate pH regulation of connexin43 channels. Biophys J 70(3):1294–1302
7. Verma V et al (2009) Novel pharmacophores of connexin43 based on the "RXP" series of Cx43-binding peptides. Circ Res 105(2):176–184
8. Verma V et al (2010) Design and characterization of the first peptidomimetic molecule that prevents acidification-induced closure of cardiac gap junctions. Heart Rhythm 7(10):1491–1498
9. Wang N et al (2013) Connexin targeting peptides as inhibitors of voltage- and intracellular Ca^{2+}-triggered Cx43 hemichannel opening. Neuropharmacology 75:506–516
10. Ponsaerts R et al (2010) Intramolecular loop/tail interactions are essential for connexin 43-hemichannel activity. FASEB J 24(11):4378–4395
11. Leybaert L et al (2017) Connexins in cardiovascular and neurovascular health and disease: pharmacological implications. Pharmacol Rev 69(4):396–478
12. De Vuyst E et al (2009) Ca^{2+} regulation of connexin 43 hemichannels in C6 glioma and glial cells. Cell Calcium 46(3):176–187
13. Kovacs M et al (2004) Mechanism of blebbistatin inhibition of myosin II. J Biol Chem 279(34):35557–35563
14. Ponsaerts R et al (2008) The myosin II ATPase inhibitor blebbistatin prevents thrombin-induced inhibition of intercellular calcium wave propagation in corneal endothelial cells. Investig Ophthalmol Vis Sci 49(11):4816–4827
15. D'Hondt C et al (2013) Negatively charged residues (Asp378 and Asp379) in the last ten amino acids of the C-terminal tail of Cx43 hemichannels are essential for loop/tail interactions. Biochem Biophys Res Commun 432(4):707–712
16. Abudara V et al (2014) The connexin43 mimetic peptide Gap19 inhibits hemichannels without altering gap junctional communication in astrocytes. Front Cell Neurosci 8:306
17. Schulz R et al (2015) Connexin 43 is an emerging therapeutic target in ischemia/reperfusion injury, cardioprotection and neuroprotection. Pharmacol Ther 153:90–106
18. Calero G et al (1998) A 17mer peptide interferes with acidification-induced uncoupling of connexin43. Circ Res 82(9):929–935
19. Iyyathurai J et al (2016) Calcium wave propagation triggered by local mechanical stimulation as a method for studying gap junctions and hemichannels. Methods Mol Biol 1437:203–211
20. Omori Y, Yamasaki H (1999) Gap junction proteins connexin32 and connexin43 partially acquire growth-suppressive function in HeLa cells by deletion of their C-terminal tails. Carcinogenesis 20(10):1913–1918
21. Siller-Jackson AJ et al (2008) Adaptation of connexin 43-hemichannel prostaglandin release to mechanical loading. J Biol Chem 283(39):26374–26382
22. D'Hondt C, Himpens B, Bultynck G (2013) Mechanical stimulation-induced calcium wave propagation in cell monolayers: the example of bovine corneal endothelial cells. J Vis Exp 77:e50443
23. Gomes P et al (2005) ATP release through connexin hemichannels in corneal endothelial cells. Investig Ophthalmol Vis Sci 46(4):1208–1218
24. D'Hondt C et al (2007) Thrombin inhibits intercellular calcium wave propagation in corneal endothelial cells by modulation of hemichannels and gap junctions. Investig Ophthalmol Vis Sci 48(1):120–133
25. De Vuyst E et al (2006) Intracellular calcium changes trigger connexin 32 hemichannel opening. EMBO J 25(1):34–44
26. D'Hondt C et al (2016) Nutrient starvation decreases Cx43 levels and limits intercellular communication in primary bovine corneal endothelial cells. J Membr Biol 249(3):363–373
27. Bol M et al (2017) At the cross-point of connexins, calcium, and ATP: blocking hemichannels inhibits vasoconstriction of rat small mesenteric arteries. Cardiovasc Res 113(2):195–206
28. Duffy HS et al (2002) pH-dependent intramolecular binding and structure involving Cx43 cytoplasmic domains. J Biol Chem 277(39):36706–36714
29. Delmar M et al (2004) Structural bases for the chemical regulation of Connexin43 channels. Cardiovasc Res 62(2):268–275
30. Marandykina A et al (2013) Regulation of connexin36 gap junction channels by n-alkanols and arachidonic acid. J Physiol 591(8):2087–2101
31. Seki A et al (2004) Modifications in the biophysical properties of connexin43 channels by a peptide of the cytoplasmic loop region. Circ Res 95(4):e22–e28
32. Retamal MA et al (2007) Cx43 hemichannels and gap junction channels in astrocytes are regulated oppositely by proinflammatory cytokines released from activated microglia. J Neurosci 27(50):13781–13792

33. Retamal MA et al (2007) Possible involvement of different connexin43 domains in plasma membrane permeabilization induced by ischemia-reperfusion. J Membr Biol 218(1–3):49–63
34. Hirst-Jensen BJ et al (2007) Characterization of the pH-dependent interaction between the gap junction protein connexin43 carboxyl terminus and cytoplasmic loop domains. J Biol Chem 282(8):5801–5813
35. Sorgen PL et al (2004) Structural changes in the carboxyl terminus of the gap junction protein connexin43 indicates signaling between binding domains for c-Src and zonula occludens-1. J Biol Chem 279(52):54695–54701
36. Gangoso E et al (2014) A cell-penetrating peptide based on the interaction between c-Src and connexin43 reverses glioma stem cell phenotype. Cell Death Dis 5:e1023
37. Omasits U et al (2014) Protter: interactive protein feature visualization and integration with experimental proteomic data. Bioinformatics 30(6):884–886